

Cloud Climatology for New Zealand and Implications for Radiation Fields

G. Pfister, R.L. McKenzie, J.B. Liley, A. Thomas

National Institute of Water and Atmospheric Research, Lauder, New Zealand

M.J. Uddstrom

National Institute of Water and Atmospheric Research, Wellington, New Zealand

A. Heidinger

NOAA/NESDIS, Office of Research and Applications, Washington DC, USA

Abstract. Work in this paper concentrates on two techniques to derive information about cloudiness. The first, all-sky imaging is used to supply cloud coverage information for a local region with high temporal resolution. Results from an all-sky camera operated in Lauder are presented and combined with global and UV irradiance measurements to work out the cloud impact on solar irradiance at the surface.

The second is a method to derive information about cloud type and microphysical parameters from AVHRR satellite measurements.

Introduction

Clouds play a critical role in regulating the amount of solar radiation penetrating the Earth's atmosphere. Factors such as cloud coverage, optical thickness, cloud geometry, liquid water content, or particle size distribution complicate a quantification of the cloud influence.

Clouds of the same type might attenuate different amounts of radiation due to variation in their micro- and macro-physical properties. Further, they may not only cause radiation values to drop below corresponding clear sky levels, but under certain circumstances may cause an increase in the solar radiation reaching the surface.

One technique to measure cloud coverage from the ground with high temporal resolution is all-sky imaging. In Lauder, New Zealand, two all-sky cameras are operated. A brief overview of the technique is presented, and the consensus between the all-sky cloud coverage and measurements of global and UV radiation is determined.

Another possibility to gain information about clouds is the analysis of satellite data. Uddstrom et al. (2000) applied a Bayesian cloud classification algorithm ("SRTex") to derive cloud type information over New Zealand from one year of high resolution NOAA14-AVHRR data. This algorithm was modified and will be applied to the complete NOAA14 data set from 1995 up to 2002 to derive a cloud climatology for New Zealand. The work has not yet finished, but the principle itself is presented.

All-Sky Imaging

In Lauder (45.04S, 169.68E, 370 m asl) two all-sky imaging systems (Long and DeLuisi, 1998) are in operation. The principles, limitations, and uncertainties of this technique, and a comparison between the two systems are described in Pfister et al. (2002).

Besides the cloud fraction (CF), the all-sky cameras deliver also an indicator for the obstruction of the sun. In general, the CF is good to about one tenth, for more than 80% of the images the two cameras agree to within 10% in cloud coverage. A comparison for the sunshine parameter shows an agreement in 90% of all images.

For the present analysis we concentrate on data from "Allsky2" (Yankee Environmental Systems Inc.), which has been in operation at Lauder since September 1999. Images are taken every minute from sunrise to sunset, and the analysis is performed over a field of view of 160°.

Cloudiness for Lauder

Allsky2 data taken over the time period July 2000 to June 2001 were used to investigate the variation in cloudiness for Lauder. For about 29% of the images the measured CF was below 10%, while in about 42% of the cases more than 90% of the sky were covered by clouds. This predominance of either "clear" or "covered" sky is also seen when looking at the frequency of occurrence for the individual months (Figure 1). Due to technical problems no data are available for October 2000.

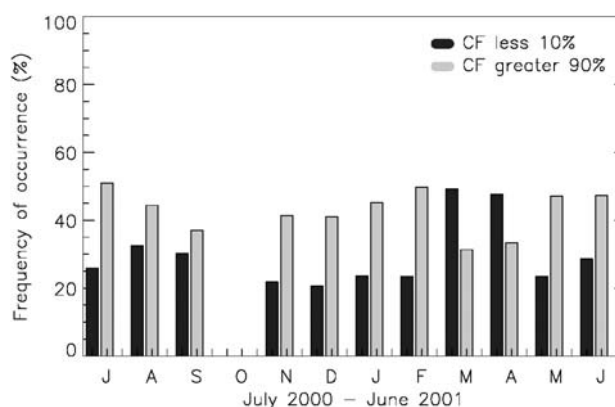


Figure 1: Monthly frequency of the occurrence of "clear sky" and "covered sky" for Lauder.

In Figure 1 a strong variation between the different months is evident. For example, in March and April the frequency of "clear sky" is larger compared to "covered sky" (i.e. ~50% compared to 30%), while in all the other months the occurrence of "covered sky" dominates. Monthly mean CF values range from 40% in March and April to 67% in July.

This monthly pattern is also reflected in the radiation data as will be shown in the next Section.

Looking at the number of clear sky days per month (CF $\leq 10\%$ for more than 90% of the day, at least 6 hours of data for a “measurements day”) we find the highest number in March (9) and April (5), none showed up for December and January. Most “cloudy days” occur for August (9) and June (7). In total, for the whole year (318 “measurement days”) we identified 37 “clear” and 41 “cloudy” days.

Influence of Clouds on Global Solar Irradiance and UV

Measurements of the global, direct, and diffuse solar irradiance performed in Lauder as part of BSRN (Baseline of Surface Radiation Network) as well as of spectral UV irradiance (McKenzie et al., 1992) were combined with the all-sky data set to investigate the cloud impact on the transfer of solar radiation through the atmosphere.

The BSRN irradiance data are available as one-minute averages, UV spectral measurements are made at every 5° change in solar zenith angle (SZA) plus at pre-set times around solar noon.

To quantify the cloud influence we refer to the ratio of measured to clear sky estimates. Clear sky values for the global irradiance were derived by fitting a curve of the form $a \cdot \cos(\text{SZA})^b$ to all clear sky measurements. For a SZA of less than 70° the fit is better than $\pm 10\%$, with 94% of the data agreeing within $\pm 5\%$.

In accordance to the monthly statistics of cloud coverage described in the earlier Section, a monthly mean measured to clear sky global irradiance ratio was calculated. Average reductions range from 18% to 33% with lowest reductions in March and April, and highest cloud impact in July 2000. The correlation between the monthly mean cloud coverage and monthly mean reduction in global irradiance is -0.9 . Nevertheless, as will be shown later, a simple relationship between CF and surface irradiance does not exist.

The erythemal UV irradiance used in the present study is taken from integrating the spectral UV measurements. For estimating clear sky UV irradiances model calculations were performed with the Tropospheric Ultraviolet Model (TUV, Version 4.1, S. Madronich, NCAR, CO, USA). The model input parameters are date and time, an average aerosol amount and surface albedo value for Lauder, and the ozone amount derived from the spectral data.

To date, UV model calculations have been performed only for the period January to April 2001. The analysis was once again restricted to SZA less than 70° to reduce the influence of measurement and modeling uncertainties.

The agreement for the UV model calculations under clear sky conditions is slightly better than for the global irradiance fit. Model and measurements agree within $\pm 5\%$. Figure 2 shows the ratio of measured to clear sky global and UV irradiances as function of the Allsky2 total cloud fraction. Data are separated into cases with the sun obscured by clouds (SO) and with the sun disk free (SF).

The obstruction of the sun disk was determined from the corresponding all-sky parameter, but, as a further check, a

data point was included only when the all-sky parameter indicated obscured (un-obscured) sun and the direct radiation was greater (less) than 120 W m^{-2} (according to WMO specifications for sunshine duration).

There is a clear separation between these two cases, although the scatter within each scenario is large, and it is obvious that an estimate of the cloud impact based on knowledge of cloud coverage and obstruction of the sun is associated with high uncertainties. Further information about the cloud type and the microphysical properties will be available from the analysis of the AVHRR data (see following Section), and is expected to allow a more detailed deduction of the consensus between cloudiness and the radiation field.

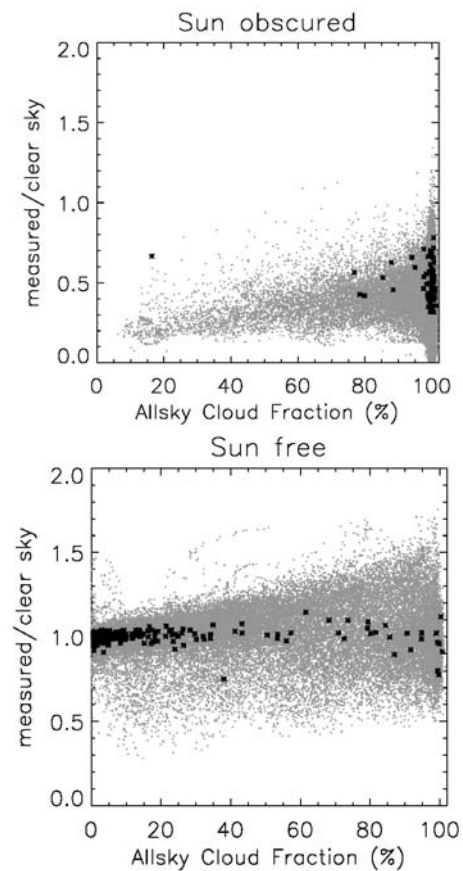


Figure 2: Ratio of measured to clear sky global irradiance (gray) and erythemal UV irradiance (black) against CF. (a) Data with the sun obscured and (b) sun not obscured.

Concentrating on the SF scenario (82245 data points for global, 490 for UV irradiance) it becomes evident, that there are numerous data points clearly exceeding expected clear sky values. Such enhancements occur when the direct radiation is nearly unaffected by clouds (un-obscured sun) and the diffuse component is increased. These situations are mainly associated with broken cloud fields and/or thin clouds near the sun. The frequency of enhanced radiation values was determined to be $\sim 5\%$ at Lauder (Pfister et al., 2002).

It can be seen that there are few data points showing a CF of nearly 100% in the SF scenario. This is either due to misclassification of the obstruction of the sun or an

overestimate of the all-sky cloud fraction.

It is also evident from Figure 2, that in the SO scenario the UV data (73 data points, 58331 data points for global irradiance) are concentrated at higher cloud fractions. This might be explained, in that integrated quantities are only derived from spectra that were not distorted by clouds during the duration of the scan. The probability that the sun disk is obscured and the radiation field varies only slightly during this time is much higher in the case of homogeneous clouds covering a large part of the sky, than in case of broken clouds and small coverage.

An interesting feature shows up when comparing the cloud impact on the global and on the UV irradiance (Figure 3). Reductions and enhancements caused by clouds are clearly less pronounced at shorter wavelengths. The same plot for the UV-A irradiance (not shown here) shows data points positioned slightly nearer to the 1:1 line, but the cloud impact is still lower compared to the whole spectral range.

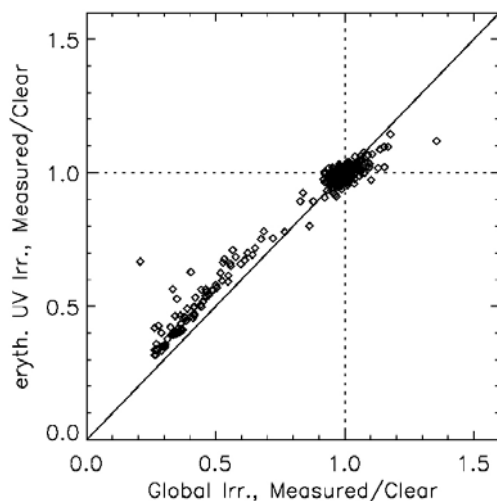


Figure 3: Ratio of measured to clear sky UV-B irradiance against measured to clear sky global irradiance.

An explanation for this result is the larger contribution of diffuse radiation at short wavelengths. For clear sky and low turbidity, the contribution of the direct to the total radiation at a SZA of 20° (70°) is about 50% (nearly zero) at 320 nm and 80% (20%) at 420 nm.

Due to this SZA dependence we also expect to find a variation in the spectral cloud impact with SZA, but this was not part of the present study.

Outlook: Cloud Climatology from AVHRR

High resolution NOAA14 AVHRR satellite data from 1995 to 2002 will be used to derive a cloud climatology for New Zealand using the Bayesian SRTex cloud classification algorithm (Uddstrom and Gray (1996), Uddstrom et al. (2000)).

SRTex follows two steps. In a first a large number of samples is labeled according to cloud type. Each sample is characterized on an 8 x 8 pixel (1.1 km resolution) tile. In the second step, the radiative and spatial data are used to specify Bayesian discriminant functions, which in turn are

applied to the satellite data.

The original SRTex code was extended by (1) adding a snow class, because the earlier version could not discriminate snow from clouds, and (2) including a retrieval algorithm for cloud optical depth (COD) and effective radius (R_{eff}) as well as aerosol optical depth over ocean (Andrew Heidinger, NOAA, personal communication). The cloud microphysical parameter will provide helpful additional information in analysing the cloud impact on surface radiation. Further information about the cloud microphysical retrieval from satellite data is found in, e.g., Nakajima and King (1990).

Figure 4 shows the Probability of Detection (POD) and the False Alarm Rate (FAR) for different cloud classes in SRTex. The discriminant model was tested by randomly separating the training samples into two subsets, using one to calculate the discriminant function, the other to check the model. Figure 4 shows the POD and FAR statistics for the different classes.

It can be seen that the distinction between no cloud and cloud has a high rate of success, but some cloud types are more often misclassified. The detection of snow gives very good results, especially when pixels are completely snow covered, but tends to give a false classification in case of partial snow cover. The skill score for the model is 75%.

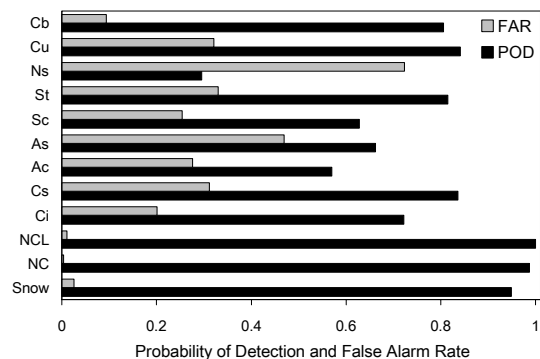


Figure 4: POD and FAR for the different cloud classes used in SRTex. NC means no cloud over sea, NCL no cloud over land. The prior probability was set to 0.1

The cloud microphysical retrieval is based on comparing measured solar reflectances with model simulations. COD and R_{eff} are inferred from solar reflection measurements at non-absorbing (e.g. channel 1, 0.55-0.68 μm) and absorbing (e.g. channel 3, 3.55-3.93 μm) wavelengths for water, while the first mainly contains information regarding COD, the latter provides knowledge about R_{eff} . For an optical depth greater than about 4-7 COD and R_{eff} can be determined nearly unambiguously (Platnick and Valero, 1995).

It must be born in mind that channel 3 is a composite of reflected and thermal radiation. To extract the solar component in this channel SRTex refers to the parameterization by Stowe et al. (1991). This approach requires the thermal emission temperature in channel 4 (10.5-11.5 μm) to be similar to that in channel 3, an

assumption that is only valid when the contribution of the thermal emission from the surface is negligible compared to that of the cloud. For this reason the retrieval is performed for optically thick clouds only (e.g. Rosenfeld and Gutman, 1994).

The model simulations for the COD and R_{eff} retrieval assume no atmosphere above the cloud top, in which case a correction should be applied to the satellite data to account for atmospheric effects. A correction is not included in the current version of SRTex, because the parameterization used to calculate the channel 3 reflectance partly corrects for the atmospheric influence, and vertical profiles of atmospheric humidity and temperature needed to correct the satellite measured reflectances are not available at sufficiently high spatial resolution.

Sensitivity studies showed, that the error in the current retrieval can be as large as 60% for COD and 85% for R_{eff} dependent on viewing geometry, cloud top altitude, atmospheric water vapor amount, and the cloud optical depth and effective radius itself. The error in R_{eff} is larger than the error in COD since the atmospheric correction for channel 3 is larger compared to channel 1.

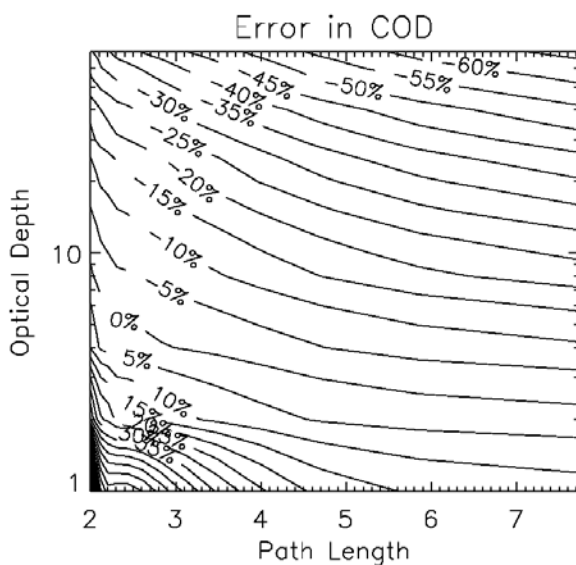


Figure 5: Error in the retrieval of COD as function of path length and COD.

Figure 5 shows as an example the error in COD as function of viewing geometry and COD if atmospheric correction is neglected. A low cloud was chosen for this example. The scan angle was varied together with the SZA in a way, that the path length of the solar photons from the sun to the cloud top and reflected back to the satellite above the cloud top varied from 2 to about 8 with atmospheric correction increasing towards higher path length.

Results will be significantly worse if the wrong thermodynamic phase for the cloud top is used (the algorithm separates ice and water clouds) or snow covered surface below the cloud is not considered.

The algorithm used currently for NOAA14 data, is

expected to give more accurate results for NOAA15 and NOAA16 AVHRR data. For these satellites a $1.6\mu\text{m}$ channel is available, which is (1) a very good discriminator for snow and water clouds, and (2) can be used in the retrieval instead of $3.5\mu\text{m}$. The correction for atmospheric influence is much smaller at $1.6\mu\text{m}$ compared to $3.5\mu\text{m}$, and a further advantage is that radiation at this wavelength is due to solar components only.

To account for snow covered surface as needed in the retrieval of COD and R_{eff} , we first apply the SRTex snow classification algorithm to winter-time satellite data, and form monthly snow maps. These in turn serve as input to the microphysical retrieval.

Data validation for the microphysical retrieval will be done by comparing COD and R_{eff} with aircraft measurements, validation of cloud coverage will be performed, e.g. by comparison with All-Sky Imaging cloud fraction.

Acknowledgements

The authors would like to thank Bruce Forgan for help with the BSRN radiation measurements and Chuck Long for support with the All-Sky cameras. Thanks are also due to Jill Scott and Mike Kotkamp for help with the operational requirements and data archival of the instruments. This work was funded under FRST contracts CO1X0033 and CO1X0032.

References

- Long, C.N. and J.J. DeLuisi, 1998. Development of an Automated Hemispheric Sky Imager for Cloud Fraction Retrievals, Proc. 10th Symp. On Meteorological Observations and Instrumentation, Phoenix, Arizona.
- McKenzie, R.L., P.V. Johnston, M. Kotkamp, A. Bittar, J.D. Hamlin, 1992. Solar ultraviolet spectroradiometry in New Zealand: Instrumentation and sample results from 1990. *Appl. Opt.*, 31, 6501, 6509.
- Nakajima, T., and M.D. King, 1990. Determination of the Optical Thickness and effective Particle Radius of Clouds from Reflected Solar Radiation Measurements. Part 1: Theory. *Atmos. Sci.*, 47, 1878-1893.
- Pfister, G., R. L. McKenzie, J. B. Liley, A. Thomas, C.N Long. B.W. Forgan, 2002. Cloud Coverage based on All-Sky Imaging and its Impact on Surface Solar Irradiance, submitted to *J. Appl. Met.*.
- Platnick, S. and F.P.J. Valero, 1995. A Validation of a Satellite Cloud Retrieval during ASTEX. *J. Atm.Sci.*, 52, 16, 2985-3001.
- Rosenfeld D. and G. Gutman, 1994. Retrieving microphysical properties near the tops of potential rain clouds by multispectral analysis of AVHRR data. *Atm. Res.*, 259-283.
- Stowe, L.L., E.P. McClain, R. Carey, P. Pellegrino, G. Gutman, P. Davis, C. Long, A. Hart, 1991. Global Distribution of Cloud Cover derived from NOAA/AVHRR operational satellite data. *Adv. Space Res.*, 11, 351-354.
- Uddstrom, M.J. and W.R. Gray, 1996. Satellite Cloud Classification and Rain-Rate Estimate using Multi-Spectral Radiances and Measures of Spectral Texture. *J. Appl. Met.*, 35, 839-858.
- Uddstrom, M.J., J.M. McGregor, W.R. Gray, J.W. Kidson, 2000. A High-Resolution Analysis of Cloud Amount and Type over Complex Topography. *J. Appl. Met.*, 40, 16-33.

